International Journal of Mechanical and Electrical Engineering
ISSN: 3005-9615 (Print), ISSN: 3005-7132 (Online) | Volume 8, Number 3, Year 2026
DOI: https://doi.org/10.62051/ijmee.v8n3.08
Journal homepage: https://wepub.org/index.php/IJMEE/index

Thermal Performance Analysis of a Triple-Tube Heat Exchanger with Internal and External Conductive Connections

Kuihua Fu

School of Ecology and Environmental, North China University of Water Resources and Electric Power, Zhengzhou, Henan, 450046, China

ABSTRACT

Latent heat storage systems are limited by the low thermal conductivity of phase change materials (PCMs), resulting in prolonged charging and discharging times. To address the issues of a single heat conduction path and thermal coupling imbalance in triplex-tube heat exchangers (TTHX), this study proposes an optimized TTHX with internal and external conductive connections. By integrating fins penetrating the tube walls at the bottom of both annular channels, a direct metallic thermal connection node is established, enabling rapid thermal equilibrium between the inner and outer HTFs. Numerical simulation results show that at an inner-to-outer ratio of 0.7, the melting time is reduced by 35.2%; at a ratio of 0.5, the solidification time is 58.9% shorter than that of the novel TTHX at the same ratio and 41.8% shorter than its optimal solidification time. The performance enhancement is attributed to multi-path heat transfer and the full development of two independent natural convection zones. This study achieves a shift from quantitative enhancement to targeted point-specific enhancement, providing new insights for the design of efficient latent heat storage systems.

KEYWORDS

Triplex-tube Heat Exchanger; Phase Change Material; Heat Transfer Enhancement; Conductive Connection; Melting and Solidification.

1. INTRODUCTION

With the gradual exhaustion of fossil fuel reserves and growing ecological concerns, nations across the globe are actively seeking efficient solutions for renewable energy utilization. Thermal energy storage systems are instrumental in combating climate change by facilitating the integration of renewable sources and mitigating the mismatch between variable energy supply and demand [1]. Nevertheless, creating affordable and high-performance thermal storage technologies continues to be a critical obstacle to the widespread implementation of renewable energy. Among the diverse thermal storage methods, latent heat thermal energy storage (LHTES) systems stand out as especially attractive, offering high energy storage capacity and nearly constant operating temperatures [2, 3].

LHTES equipment with solid-liquid phase change is indispensable for addressing the mismatch between renewable energy supply and demand. The primary challenge limiting LHTES system effectiveness stems from the low thermal conductivity of phase change materials (PCMs), resulting in prolonged charging/discharging times to reach design thermal storage capacity. Consequently, numerous investigations have been conducted to enhance the heat transfer rate [2-4]. The main structural types of LHTES devices include shell-and-tube, plate, and heat-pipe types. The shell-and-tube type can be divided into concentric/eccentric double/triple/multi-tube heat exchangers [4]. The tube geometries can be cylindrical, spiral, or other complex configurations [4,5]. The main layout

orientations are vertical and horizontal. Among shell-and-tube LHTES heat exchangers, the triplex-tube heat exchanger (TTHX) is favored for its unique advantages. It provides enhanced surface area for heat transfer between the heat transfer fluid (HTF) and PCM while maintaining geometrical simplicity and superior pressure resistance.

The classic structure of TTHX features PCM filled in the middle annulus and HTF flowing through the inner tube and outer annulus, referred to as the conventional TTHX. This configuration was first proposed by Basal and Ünal in 2013 [6], and its thermal performance is significantly superior to that of the double-tube heat exchangers [6-8]。Researchers have conducted numerous studies to enhance the heat transfer rate of conventional TTHX. Leong et al. [9] comprehensively reviewed enhancement techniques to reduce the melting and solidification time of TTHX. The enhancement techniques include fin design and optimization, nano-enhanced PCM, micro-encapsulation, metal foam matrices, and geometric modifications.

Enhancing heat transfer through reversed configuration PCM: Heat-transfer enhancement via reversed arrangement PCM of TTHXs (hereinafter termed new TTHXs) has emerged as a promising approach [10-12]. In the new TTHX, PCM is filled in the inner tube and outer annular regions, while HTF flows through the center annular region. Gorzin et al. [10] first investigated the new TTHX, demonstrating that distributing 40% of the PCM mass in the inner tube and 60% in the outer annular region reduced melting time by 52% compared with double-tube heat exchangers with external PCM filling. Sriram and Bhattacharya [11] analyzed the influence of inner tube diameter on complete melting time under identical PCM volume and HTF mass flow rate conditions. Their findings revealed an optimal inner tube diameter that significantly accelerated melting rates compared to conventional double-tube systems. Furthermore, Hussain et al. [12] investigated the heat transfer enhancement through branched fin integration in the outer annulus of a new TTHX, finding that optimized branched fin configurations reduced melting time by 35% compared to rectangular fin designs. Although new TTHXs feature larger heat transfer areas than conventional configurations, the correlation between increased surface area and superior thermal performance remains unclear. Notably, enlarged heat transfer surface area do not necessarily enhance melting and solidification rates, as the purely conductive regions occurring during later melting stages may compromise overall performance [13].

The above reviews show that although previous studies have demonstrated that both new and conventional TTHXs outperform double-tube designs in melting rates [6, 8, 10, 11], a critical knowledge gap persists. Existing research still exhibits significant limitations, including a single heat conduction path dominated by tube wall thermal resistance, thermal coupling imbalance between the inner/outer annular channels and the PCM layer, and the difficulty in balancing enhanced heat transfer with flow resistance. This study provides a comprehensive analysis of the thermal performance of the novel triple-tube heat exchanger, systematically examines the influence of internal and external conductive connections on its thermal performance, and deeply reveals the underlying heat transfer mechanisms that enhance heat transfer. The main novel contributions of this work are:

(1) By simultaneously integrating fins that penetrate the tube wall at the bottom of both the inner and outer annular channels, a direct metallic thermal connection node between the inner and outer flow channels was established. This structural innovation enables rapid thermal equilibrium between the inner and outer HTFs at the bottom, breaking the path limitation of relying solely on indirect heat exchange via the PCM in traditional structures, and significantly enhancing the synergy of bilateral heat transfer.

(2) It was demonstrated that in heat exchanger design, more fins do not necessarily lead to better performance. Instead, significant performance improvements can be achieved by identifying the critical paths of temperature response and implementing targeted enhancement at key locations. This provides a new theoretical approach for the optimized design of phase change energy storage heat exchangers.

The remainder of this paper is organized as follows. Section 2 introduces the physical and mathematical models, Section 3 compares the thermal performance of the internal and external conductive connection and the novel TTHX, and Section 4 summarizes the study. To address these critical gaps, this study conducts a comprehensive analysis of the thermal performance of the TTHX and reveals the underlying heat transfer mechanisms. This work enhances the understanding of the fundamental mechanisms and lays the groundwork for innovative design strategies for efficient latent heat storage systems.

2. TTHX STRUCTURES

2.1. Physical Model

The internal and external conductive connection and the TTHX with PCM arranged inside and outside are shown in Figure 1. The inner tube, middle tube, and outer tube of both the internal and external conductive connection and the TTHX with PCM arranged inside and outside are metallic. Although the temperature of the HTF varies along the axial direction, the temperature variation is minimal [11]. Therefore, the 3D model of the TTHX device is simplified to a 2D model to reduce computational complexity. Although this simplification is a compromise, it allows for a valid performance comparison.

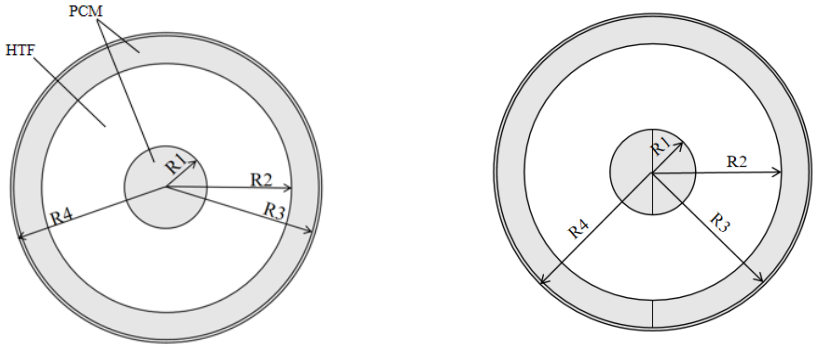

Fig 1. Schematic diagram of the horizontal TTHX: (left) PCM arranged inside and outside, (right) internal and external conductive connection.

Table 1. Thermophysical properties of paraffin RT50 and pipe wall material [14]

Parameters	PCM RT50	PCM RT82	Polystyrene	Copper	Aluminum
Solidus density (ρ_s), kg/m^3	880	950	1040	8978	2719
Liquidus density (ρ_l), kg/m^3	760	770	/	/	/
Specific heat capacity (C_p), J/(kg·K)	2000	2000	1300	381	871
Latent heat (L), kJ/kg	168	176	/	/	/
Melting temperature (T), K	318.15–324.15	351.15-355.15	/	/	/
Thermal conductivity (λ), W/(m·K)	0.20	0.2	0.03	387.6	202.4
Thermal expansion coefficient (α), 1/K	0.0006	0.001	/	/	/
Dynamic viscosity ($\boldsymbol{\mu}$), N·s/m^2	0.03	0.03	/	/	/

The use of metallic outer tubes, such as copper, is common in most studies. However, using non-metallic outer tubes, such as polystyrene, which has low thermal conductivity, can reduce heat loss, equipment weight and cost. Therefore, both outer tube materials are considered in this study. The wall thickness of metallic tubes is set to 1.0 mm, with the thermal resistances of the inner and middle

tube walls considered negligible due to their thin wall and high thermal conductivity. Consequently, the effect of the inner tube wall thickness is ignored in the simulations. When the outer tube is made of polystyrene, its thermal conductivity is negligible, while for metallic tubes, heat conduction along the circumferential direction should be considered. The inner, middle, and outer radii are denoted as R1, R2, and R3, respectively. The inner diameter of the outer tube and the PCM mass remain constant across all cases. The inner–outer PCM ratio is used to denote the different structural forms of new TTHXs. Paraffin RT50 is selected as the PCM. The thermophysical properties of the PCM and the outer tube material are shown in Table 1.

2.2. Mathematical Model

2.2.1. Governing Equations

The melting and solidification models are utilized to deal with charging and discharging heat transfer processes based on the finite volume and enthalpy-porosity technique. To facilitate numerical computations, the following assumptions are adopted:

(1) PCM exhibits uniform distribution and isotropic properties [11].

(2) Liquid PCM flow is laminar, transient, and incompressible [10,11].

(3) Heat losses to the ambient environment are neglected owing to effective insulation [10,11].

(4) PCM density variations are evaluated using the Boussinesq approximation to capture buoyancy-driven effects, while other thermophysical properties remain constant [10,11].

(5) Volume expansion, viscous dissipation, and interfacial thermal resistance are negligible [10,11].

Based on the above assumptions, continuity, momentum, and energy equations are developed as follows:

Continuity equation**:**

$$\frac{\partial_{\rho}}{\partial \tau}+\frac{\partial(\rho u)}{\partial x}+\frac{\partial(\rho v)}{\partial y}=0 \tag{1}$$

where ρ denotes PCM density, τ is time, u and v are velocities in the x direction and y direction, respectively.

Momentum equations [15, 16]**:**

$$\frac{\partial(\rho u)}{\partial \tau}+u\frac{\partial(\rho u)}{\partial x}+v\frac{\partial(\rho u)}{\partial y}=-\frac{\partial p}{\partial x}+\mu\left(\frac{\partial^2 u}{\partial x^2}+\frac{\partial^2 u}{\partial y^2}\right)-\frac{C(1-\beta)^2}{\beta^3+\varepsilon}u \tag{2}$$

$$\frac{\partial(\rho v)}{\partial \tau}+u\frac{\partial(\rho v)}{\partial x}+v\frac{\partial(\rho v)}{\partial y}=-\frac{\partial p}{\partial y}+\mu\left(\frac{\partial^2 v}{\partial x^2}+\frac{\partial^2 v}{\partial y^2}\right)+\rho g-\frac{C(1-\beta)^2}{\beta^3+\varepsilon}v \tag{3}$$

where p denotes pressure, μ represents dynamic viscosity, g is gravitational acceleration, β is the liquid fraction of the melted PCM, C is the mushy zone constant (10^5 kg·s^{-1}·m^{-3}), and ε is a small constant (0.0001) to avoid division by zero. The phase change behavior within the mushy zone is captured using the enthalpy-porosity formulation implemented in ANSYS Fluent, wherein each computational cell is treated as a porous medium with porosity equivalent to the local liquid fraction β.

$$\beta=\begin{cases}0 & T<T_s\\ \frac{T-T_s}{T_l-T_s} & T_s\le T\le T_l\\ 1 & T>T_l\end{cases} \tag{4}$$

where T is the PCM temperature, T_s is the solidus temperature, and T_l is the liquidus temperature.

When $\beta = 0$, velocity is completely suppressed, corresponding to the solid phase. When $\beta = 1$, full fluid motion is allowed, corresponding to the liquid phase. Within the intermediate mushy region where $0 < \beta < 1$, flow resistance varies continuously as a function of liquid fraction, enabling a smooth modeling of phase transition and natural convection within the PCM domain.

The density of the molten PCM is governed by both pressure and temperature variations. However, owing to negligible pressure fluctuations during the melting process, temperature gradients constitute the predominant driving mechanism for natural convection. To accurately capture this thermally-induced convection, the Boussinesq approximation is implemented. This approximation treats density as constant throughout all terms in the momentum equation, with the exception of the buoyancy term, where density variations are assumed to depend exclusively on temperature. These thermally-induced density variations serve as the principal contributor to buoyancy forces, thereby providing an accurate representation of natural convection within the molten region. Consequently, the density ρ appearing in the buoyancy term of the momentum equation is typically approximated as [4]:

$$\rho = \rho_m[1 - \alpha(T - T_m)] \tag{5}$$

where T_m is the mean melting temperature, ρ_m is the corresponding density at T_m, T is the PCM temperature, and α is the thermal expansion coefficient.

Energy equation:

Given that the enthalpy method effectively circumvents the computational complexities associated with tracking moving phase interfaces in conventional energy balance formulations, this approach is implemented for energy conservation analysis, expressed as follows:

$$\frac{\partial(\rho H)}{\partial \tau} + u\frac{\partial(\rho H)}{\partial x} + v\frac{\partial(\rho H)}{\partial y} = \lambda \cdot \left(\frac{\partial^2 T}{\partial x^2} + \frac{\partial^2 T}{\partial y^2}\right) \tag{6}$$

where λ is the thermal conductivity, and H is the total volumetric enthalpy of PCM, a sum of sensitive enthalpy h and latent heat of enthalpy ΔH.

$$H = h + \Delta H \tag{7}$$

$$h = h_\mathrm{ref} + \int_{T_\mathrm{ref}}^{T} c_p\, dT \tag{8}$$

$$\Delta H = \beta L \tag{9}$$

where C_p is the constant pressure-specific heat, h_{ref} is the reference sensitive enthalpy at T_{ref} = 300.15 K, and L is the latent heat of fusion.

2.2.2. Boundary and Initial Conditions

Appropriate boundary and initial conditions are crucial for accurate numerical simulation. For the 2D simplified model presented in Fig. 1, the wall temperatures of inner and middle pipes are assumed to approximate the HTF temperature for computational efficiency, while the outer pipe wall surface is treated as adiabatic boundary owing to effective thermal insulation. For the melting process, the PCM initial temperature is prescribed as 300.15 K to ensure a completely solid initial state, while the HTF temperature is 353.15 K. Conversely, for the solidification process, the PCM initial temperature is prescribed as 353.15 K to maintain a fully liquid initial state, while HTF temperature is 300.15 K. The thermal resistances of the inner and middle pipe walls are neglected due to their negligible thermal resistance. A no-slip boundary condition is imposed at all wall-PCM interfaces.

2.2.3. Numerical Methods

The melting/solidification model embedded within ANSYS Fluent 2019R2 is employed to simulate the thermal behavior of the PCM. The enthalpy-porosity method is implemented to model the phase change process by tracking the liquid fraction within each computational cell, rather than explicitly capturing the moving phase interface [17]. A pressure-based solver is utilized, which is well-suited for slow-moving, incompressible fluid flows. The SIMPLE algorithm is employed for pressure-velocity coupling. The pressure gradient is discretized using the standard scheme, while the momentum and energy equations are discretized using the second-order upwind difference scheme to ensure numerical accuracy. Convergence criteria are established as 10^{-6} for the energy equation, and 10^{-4} for the momentum and continuity equations. The under-relaxation factors are set as follows: momentum 0.7, pressure correction 0.3, density 1, liquid fraction 0.9, and energy 1.； To monitor the overall phase change progression and thermal response, the area-weighted average liquid fraction and mean temperature of the PCM domain are recorded as functions of time.

3. INTERNAL AND EXTERNAL CONNECTION

In previous studies, where PCM was arranged inside and outside the TTHX, the single heat transfer path resulted in a significant difference between melting and solidification times. Therefore, in this section, the inner and outer tubes are connected on both sides, and 1 mm copper fins have been integrated onto the outer walls of both the inner and outer tubes. These inner and outer fins form a continuous heat conduction path in order to reduce the disparity between melting and solidification.

3.1. Meting Process

The inner–outer PCM ratio plays a decisive role in determining the overall thermal performance of the new TTHX. When the inner and outer PCM regions reach complete melting or solidification simultaneously, namely β=1 or β=0, the system melting or solidification time is minimized. To identify the optimal geometric configuration, six different inner–outer PCM volume ratios are examined at constant external dimensions and total PCM volume. The geometric parameters of the PCM are shown in Table 2.

Based on the geometric parameters summarized in Table 2, numerical simulations were conducted for different inner-to-outer ratios using the aforementioned method. The corresponding melting times for the internal and external conductive connections and the novel TTHX are shown in Figure 2.

Table 2. Geometric parameters for Internal and external connection and new TTHXs.

Item		Inner radius (mm)	Middle radius (mm)	Outer radius (mm)
Inner–outer PCM volume ratios	0.3	33.90	78.54	100
	0.4	37.72	80.27	100
	0.5	40.74	81.73	100
	0.6	43.21	82.99	100
	0.7	45.28	84.09	100
	0.8	47.05	85.05	100

Figure 2 shows that the melting time curves for both the internal and external conductive connection and the novel TTHX initially decrease and then increase. When the optimal inner-to-outer ratio is 0.7, the melting time for both structures is the shortest, with the melting time for the internal tube conductive connection being 35.2% shorter than that of the novel TTHX.

To investigate the heat transfer mechanism leading to the slower melting of the novel TTHX, Figure 3 presents the melting contour maps for the internal and external conductive connection and the novel TTHX at an inner-to-outer ratio of 0.7.

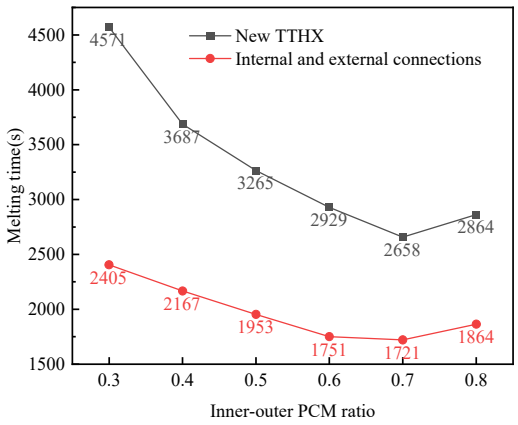

Fig 2. Comparison of melting time

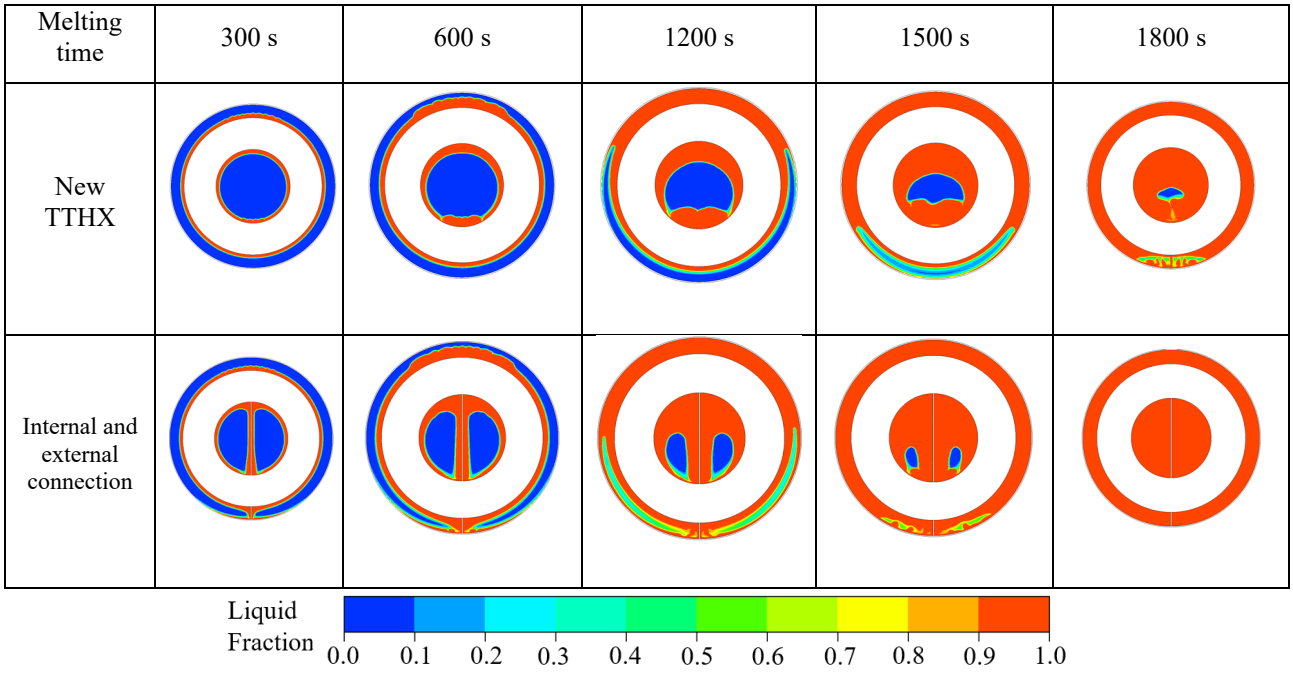

Fig 3. Comparison of melting cloud maps

Figure 3 shows that for the novel TTHX, the upper region of the PCM module melts first due to natural convection during the melting process. However, for the internal and external conductive connection, the bottom section leverages its fins to establish an efficient heat conduction path, allowing heat to be preferentially transferred to the phase change material region at the bottom of the outer ring. This enables melting to commence simultaneously at both the top and bottom. Additionally, conductive paths are also constructed internally, forming two relatively independent natural convection zones. This separation allows natural convection to develop more fully within each zone, resulting in more significant convection intensity.

The variation trends of liquid fraction and temperature are shown in Fig. 4.

Figure 4 indicates that the melting performance of the internal and external conductive connection is significantly superior to that of the TTHX with PCM arranged inside and outside, demonstrating that this optimization method is feasible.

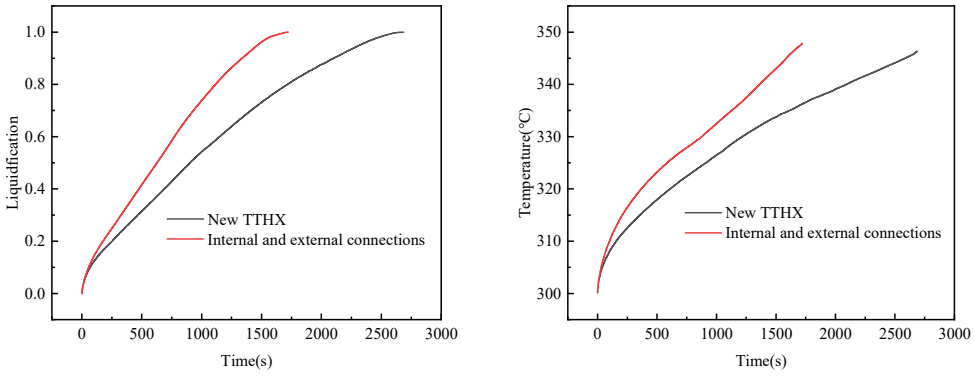

Fig 4. Thermal performance comparison

3.2. Solidification Process

Similarly, using the same boundary and initial conditions as described in Section 2.2.3, simulations were performed to investigate the solidification process of the internal and external conductive connection and the novel TTHX under different configurations. Figure 5 compares the corresponding solidification times of the two.

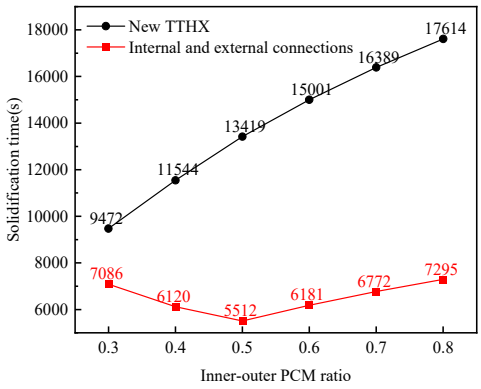

Fig 5. Comparison of solidification time

Figure 5 shows that the novel TTHX achieves the shortest solidification time at a ratio of 0.3, while the internal and external conductive connection reaches its minimum solidification time at a ratio of 0.5, which is 41.8% shorter than the optimal solidification time of the novel TTHX and 58.9% shorter than the solidification time of the novel TTHX at the same ratio. Although the melting time increases correspondingly with a decreasing fill ratio, when the ratio decreases from 0.7 to 0.3, the melting time of the metal outer tube structure increases by 1913 s, while for the internal and external conductive connection, when the ratio decreases from 0.7 to 0.5, the melting time increases by only 232 s. Therefore, the melting and solidification times of the internal and external conductive connection structure are less affected by the fill ratio of the internal and external PCM, which fully demonstrates the better stability of this structure.

To gain insight into the heat transfer mechanism of the solidification process, Figure 6 compares the solidification contour maps of the internal and external conductive connection and the novel TTHX at ratios of 0.5 and 0.3.

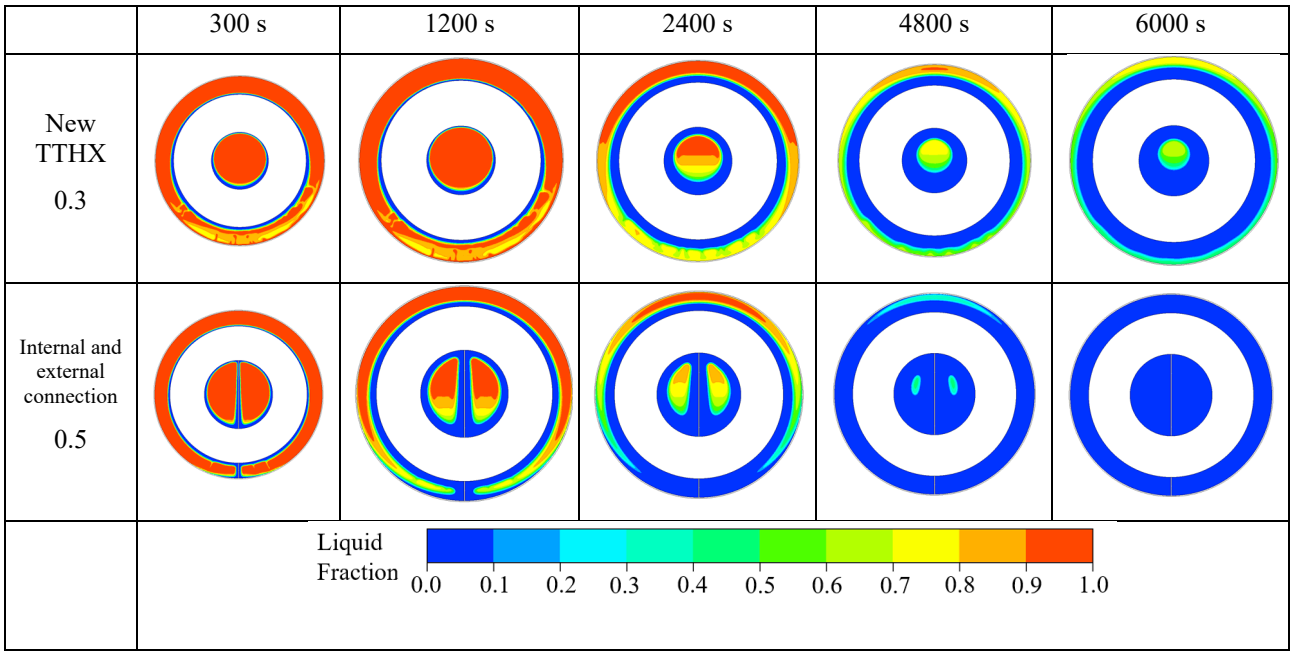

Fig 6. Solidification clouds for different PCM configurations

Figure 6 illustrates that, as the solidification process is primarily controlled by heat conduction, the novel TTHX can only transfer heat through the tube walls. In contrast, the internal and external conductive connection enables multi-path heat transfer via the heat conduction paths formed by the fins. Consequently, the solidification process is significantly faster than that of the novel TTHX.

To gain further insights into the influence of PCM layout on the thermal release performance of the TTHX, the comparative results of thermal performance during the solidification process are presented in Fig. 7.

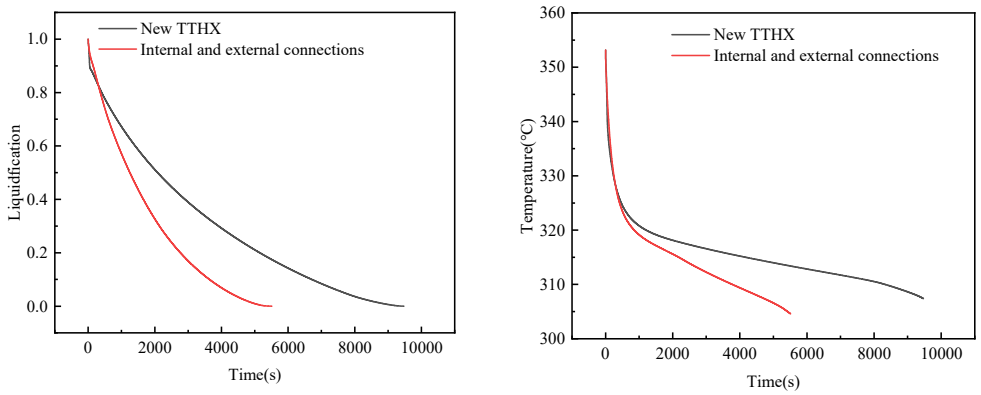

Fig 7. Thermal performance of solidification versus time

Figure 7 indicates that at the very beginning of the solidification process, the difference in solidification performance between the two configurations is minimal. However, once the heat conduction path established by the internal and external conductive connection begins to transfer heat, the outer metal wall also starts to participate in heat transfer after the PCM at the bottom has solidified. In contrast, the outer metal wall of the novel TTHX is unable to transfer heat effectively because it has not yet come into contact with solidified PCM. Therefore, the impact of the internal and external conductive connection on the solidification process is significantly greater than its impact on the melting process.

4. CONCLUSION

This study conducts a comparative analysis of the melting and solidification performance between the internal and external conductive connection and the novel TTHX. The main conclusions regarding the TTHX with internal and external conductive connection are as follows:

The TTHX with internal and external conductive connection significantly enhances melting and solidification performance through the construction of heat conduction paths via fin connections. When the inner-to-outer ratio is 0.7, the melting time is reduced by 35.2%. When the inner-to-outer ratio is 0.5, the solidification time is 58.9% shorter than that of the novel TTHX at the same ratio and 41.8% shorter than the optimal solidification time.

This study demonstrates that in phase change material-based thermal storage systems, combining increased heat transfer area with enhanced thermal conduction in the most unfavorable regions is key to achieving significant performance improvements. This approach represents a shift from increasing surface area to implanting critical paths, achieving substantial performance gains with a minimalist structure. At the mechanistic level, it reveals the directional heat conduction effect of a single penetrating fin, offering both theoretical innovation and practical engineering guidance.

DECLARATION OF INTEREST STATEMENT

The authors declare that they have no known competing financial interests or personal relationships that could have appeared to influence the work reported in this paper.

REFERENCES

[1] L. Vallese, H. Javadi, B. Badenes, J. F. Urchueguia, G. Lombardo, D. Menegazzo, et al., A comprehensive review of thermal energy storage technologies and their applications: Creation of a database, Renew Sust Energ Rev 225 (2026) 116133. https://doi.org/10.1016/j.rser.2025.116133.

[2] H. Togun, H. S. Sultan, H. I. Mohammed, A. M. Sadeq, N. Biswas, H. A. Hasan, et al., A critical review on phase change materials (PCM) based heat exchanger: Different hybrid techniques for the enhancement, J Energy Storage 79 (2024) 109840. https://doi.org/10.1016/j.est.2023.109840.

[3] Z. Chang, K. Wang, X. Wu, G. Lei, Q. Wang, H. Liu, et al., Review on the preparation and performance of paraffin-based phase change microcapsules for heat storage, J Energy Storage 46 (2022) 103840. https://doi.org/10. 1016/j. est.2021.103840.

[4] M. Wang, W. Liu, J. Wang, J. Xu, Research progress of shell-and-tube heat exchanger of latent heat storage (in Chinese), J Eng Therm Energy Power 38 (2023) 1 – 12. https://doi.org/10.16146/j.cnki.rndlgc.2023.10.001.

[5] B. Kurşun, M. Balta, K. Karabulut, Exploring the impact of inner and middle channel geometries on the melting rate of PCM-metal foam composition in a triplex tube heat exchanger, Therm Sci Eng Prog 51 (2024) 102621. Https://doi.org/10.1016/j.tsep.2024. 102621.

[6] B. Basal, A. Ünal, Numerical evaluation of a triple concentric-tube latent heat thermal energy storage. Sol Energy, 92 (2013) 196 –205. https://doi.org/10.1016/j.solener.2013.02.032.

[7] R. Eibahjaoui, H. E. Qarnia, A. Naimi, Thermal performances analysis of combined solar collector with triple concentric-tube latent heat storage systems, Energ Buildings 168 (2018) 438 – 456. https://doi.org/ 10.1016/j. enbuild. 2018.02.055.

[8] G. Chen, G. Sun, D. Jiang, Y. Su, Experimental and numerical investigation of the latent heat thermal storage unit with PCM packing at the inner side of a tube, Int J Heat and Mass Tran 152 (2020) 119480. https://doi. org/ 10. 1016/j.ijheatmasstransfer.2020.119480.

[9] K. Y. Leong, S. Hasbi, B. A. Gurunatha, State of art review on the solidification and melting characteristics of phase change material in triplex-tube thermal energy storage, J Energy Storage 41 (2021) 102932. https://doi. org/10. 1016/ j.est. 2021.102932.

[10] M. Gorzin, M. J. Hosseinib, A. A. Ranjbar, R. Bahrampoury, Investigation of PCM charging for the energy saving of domestic hot water system, Appl Therm Eng 137 (2018) 659 – 668. https://doi.org/ 10.1016/j. applthermaleng. 2018.04.016.

[11] M. Sriram, A. Bhattacharya, Analysis and optimization of triple tube phase change material based energy storage system, J Energy Storage 36 (2021) 102350. https://doi.org/10.1016/j.est.2021.102350.

[12] B. Hussain, M. Irfan, M. M. Khan, S. Ullah, F. Hasnain, Geometric optimization of fin structures for accelerated melting of phase change material in a triplex tube heat exchanger, J Energy Storage 79 (2024) 110162. https://doi.org/10.1016/j.est.2023.110162.

[13] M. M. Zaytoun, M. M. El-Bashouty, M. M. Sorour, M. A. Alnakeeb, Heat transfer characteristics of PCM inside a modified design of shell and tube latent heat thermal energy storage unit, Case stud therm Eng 49 (2023) 103372. https://doi.org/10.1016/j.csite. 2023.103372.

[14] S. Seddegh, X. Wang, A. D. Henderson, A comparative study of thermal behavior of a horizontal and vertical shell-and-tube energy storage using phase change materials, Appl Therm Eng 93 (2016) 348 – 358. https://doi.org/ 10. 1016/j. applthermaleng.2015.09.107.

[15] M. Wang, X. Dou, W. Liu, K. Fu, Enhanced thermal performance of a multi-module latent heat storage heat exchanger with mesh-like flow channels, Energy 334 (2025) 137857. https://doi.org/10.1016/j.energy.2025.137857.

[16] M. Mozafari, A. Lee, S. Cheng, A novel dual-PCM configuration to improve simultaneous energy storage and recovery in a triplex-tube heat exchanger, Int J Heat Mass Transf 186 (2022) 122420. https://doi.org/ 10. 1016/ j. ijheatmasstransfer.2021.122420.

[17] M. Wang, W. Liu, Thermal performance analysis of a new multiple flat-plate latent heat storage heat exchanger, J Energy Storage 98 (2024) 113035. https://doi.org/10.1016/j.est.2024.113035.